Vol 18 No 8, August 2009
1674-1056/2009/18(08)/3384-11

Chinese Physics B

© 2009 Chin. Phys. Soc.
and IOP Publishing Ltd

Experimental study of highly excited even-parity bound states of the Sm atom*

Qin Wen-Jie(秦文杰), Dai Chang-Jian(戴长建)†,
Xiao Ying(肖 颖), and Zhao Hong-Ying(赵洪英)

Key Laboratory of Display Materials and Photoelectric Devices, Ministry of Education, Tianjin 300384, *China*

School of Science, Tianjin University of Technology, Tianjin 300384, *China*

(Received 18 December 2008; revised manuscript received 16 February 2008)

In this work, a three-step autoionization detection method and direct photoionization detection method are employed to measure the highly excited even-parity states of the Sm atom in the energy region between 36360 cm^{-1} and 40800 cm^{-1}. Comparisons between the results from the two detection techniques enable us to discriminate the Rydberg states from the valence states in the same energy region with the information of level energies, possible J values and their relative intensities. Furthermore, in the experiment two different excitation schemes are designed to obtain the spectra of highly excited even-parity states of the Sm atom. With a detailed analysis of the experimental data, this work not only confirms the results about many spectral data from the literature with different excitation schemes, but also reports new spectral data on 29 Rydberg states and 23 valence states.

Keywords: Rydberg state, valence state, Sm atom
PACC: 3280, 3150, 3280F

1. Introduction

With the development of the tunable laser, much more information about highly excited states of atoms can be obtained by laser spectroscopy, as compared with the traditional emission and absorption spectroscopy.[1−3] Especially, due to the importance of highly-excited states of complex atoms for both fundamental and applied physics, not only have the spectra of alkaline-earth atoms been studied in the last two decades,[4−8] but also the investigation of the rare-earth atoms has become an interesting aspect recently.[9−11]

Among the rare-earth atoms, the spectrum of the Yb atom has been studied the most due to its completely filled $4f$ shell.[12−14] With only two s-electrons outside the closed shell, the spectrum of the Yb atom is very similar to those of alkaline-earth atoms. However, the spectrum of the Sm atom is much more complex due to its very unstable $4f$ shell and very complicated structure of the ground state. Obviously, the fine structures of the ground state $4f^6 6s^2\ ^7F_{0-6}$ can be readily populated as the Sm metal is heated to produce an atomic beam. Namely, the thermal populations of the seven fine-structure states are 21% ($^7F_0$), 37.8% ($^7F_1$), 25.5% ($^7F_2$), 10.9% ($^7F_3$), 3.6% ($^7F_4$), 1% ($^7F_5$) and 0.2% ($^7F_6$), respectively, according to the Boltzmann distribution. The thermal population may cause two serious consequences in the experiment: first, the number of atoms in a given initial state is reduced significantly, thus weakening the strength of the transition signal; secondly, one photon from the first laser may drive several transitions from different initial states, making the spectrum a mixed picture of many transitions, which is very difficult to analyze. The difficulties mentioned above have had the consequence that only a few studies on highly excited even-parity states of the Sm atom have been reported.[15−18] Moreover, these investigations have not provided information about the relative intensities of transitions in their observed spectra, and could not discriminate the Rydberg states from the valence states in the same energy region.

Recently, the autoionization detection method was introduced to detect Rydberg states in which they are determined by driving the atoms to autoionizing

*Project supported by the National Natural Science Foundation of China (Grant Nos 10574098 and 10674102) and the Natural Science Foundation of Tianjin (Grant No 05YFJMJC05200).
†Corresponding author. E-mail: daicj@126.com

states and detecting the ions originating from the autoionization process. This method has been utilized to study the even-parity Rydberg levels of alkaline-earth atoms,[19−21] and has been proved much more versatile in detecting both the low-lying and high-lying members of Rydberg states than the other conventional detection methods.[22−24] In this paper, the same method is applied to the Sm atom to verify its validity in more complicated atoms. With a detailed analysis of the data, we not only report many new spectral data but also identify a large number of even-parity Rydberg states that are discriminated from the valence states in the same energy region. These experimental data are very useful for many purposes, such as laser isotope separation and theoretical calculation of the atomic structure of the Sm atom.

In the following text, an introduction to the experimental details will be given in Section 2; the experimental results and discussion are presented in Section 3, and Section 4 gives the main conclusions.

2. Experiment

The experimental apparatus used in this work is illustrated in Fig.1. Three tunable dye lasers with widths of 0.1 cm^{-1} are pumped by the second or third harmonics of a Giant-770 model Nd:YAG pulsed laser with pulse duration 6–8 ns running at 20 Hz. The atomic beam of Sm is produced from a resistively heated oven inside a vacuum chamber with an environment of 1.5×10^{-4} Pa. The atomic beam is collimated to avoid Doppler broadening, and directed to a region between two electric field plates, 1 cm apart, where it is crossed perpendicularly by the two or three laser beams for direct photoionization detection and autoionization detection. After a time delay of 500 ns to the laser pulse, a 100 V pulsed electric field is applied to the plates in order to drive the ions resulting from autoionizing decay into a microchannel plate (MCP) detector. The signal pulses are integrated by a boxcar averager and stored in a computer for further analysis.

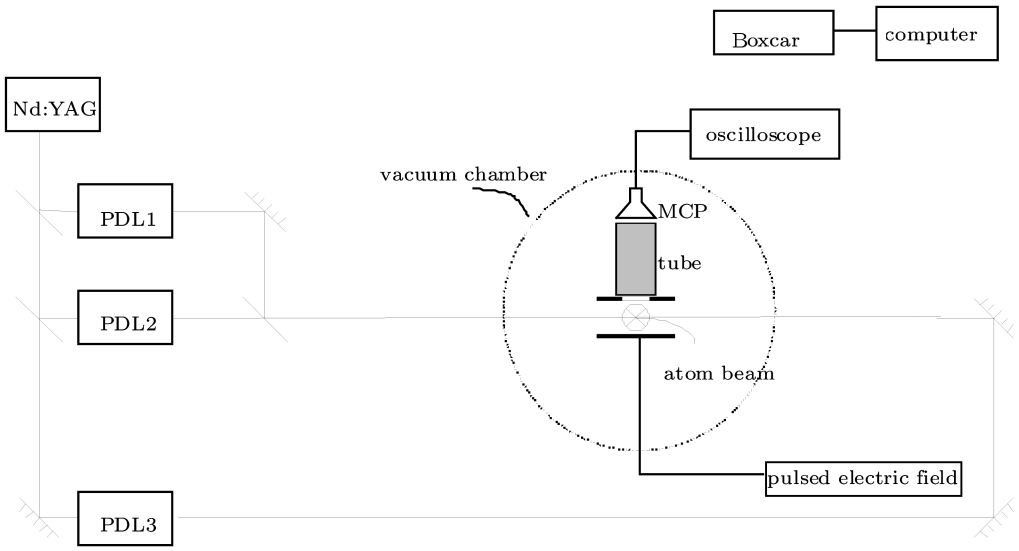


Fig.1. Schematic diagram of the experimental apparatus. It includes the excitation lasers (PDL: pulsed dye laser), the atomic beam and the detection analysis systems. The atomic beam is produced in the vacuum chamber. The ion signal is detected by an MCP, averaged by a boxcar and stored in a computer for further analysis.

As mentioned above, the extraordinarily complicated energy structures may involve a great number of doubly excited valence states, such as $4f^5 5d6s6p$ configurations, below the first ionization limit. These valence states have a shorter lifetime, converging to the higher ionization limit. In order to investigate the highly excited even-parity states of the Sm atom systematically, two different detection methods, autoionization detection and direct photoionization detection, are employed. On the other hand, it is apparent that at working temperature, a significant population should exist in the $^7F_1$ atomic state whose energy is only 292.58 cm^{-1} above the ground state.[25] That is, one is likely to obtain a strong signal if one chooses the $^7F_1$ atomic state as the initial state for the first-step excitation. Keeping this information in mind, the highly excited even-parity states can be

detected with both autoionization and direct photoionization detection methods. In each case, the wavelength of the first laser can be fixed at two values depending on which excitation schemes are chosen. In the case of autoionization detection, the following two different excitation schemes are employed:

(a) $4f^6 6s^2[^7F_1] \xrightarrow{\lambda_1} 4f^6 6s6p[^7D_2] \xrightarrow{\lambda_2} 4f^6 6snl \xrightarrow{\lambda_3} 4f^6 6pnl(4f^5 5d6snl)$,

(b) $4f^6 6s^2[^7F_1] \xrightarrow{\lambda_1'} 4f^6 6s6p[^7F_0] \xrightarrow{\lambda_2'} 4f^6 6snl \xrightarrow{\lambda_3'} 4f^6 6pnl(4f^5 5d6snl)$.

Similarly, in the case of direct photoionization detection the two excitation schemes are as follows:

(a) $4f^6 6s^2[^7F_1] \xrightarrow{\lambda_1} 4f^6 6s6p[^7D_2] \xrightarrow{\lambda_2} 4f^6 6snl(4f^5 5d6s6p) \xrightarrow{\lambda_2}$ continuum state,

(b) $4f^6 6s^2[^7F_1] \xrightarrow{\lambda_1'} 4f^6 6s6p[^7F_0] \xrightarrow{\lambda_2'} 4f^6 6snl(4f^5 5d6s6p) \xrightarrow{\lambda_2'}$ continuum state,

where l can be 0 and 2, respectively. Information about the initial state, the intermediate states and the possible final states is also given. In scheme (a), the wavelength of the first laser λ_1 is fixed at 464.67 nm to excite the Sm atom from the $4f^6 6s^2[^7F_1]$ initial state to the $4f^6 6s6p[^7D_2]$ intermediate state. In scheme (b), the wavelength of the first laser λ_1' is fixed at 570.83 nm to excite the Sm atom from the $4f^6 6s^2[^7F_1]$ initial state to the $4f^6 6s6p[^7F_0]$ intermediate state. In both schemes, the wavelength of the second laser is scanned to excite the atoms to $4f^6 6snl$ Rydberg states and doubly excited $4f^5 5d6s6p$ valence states.

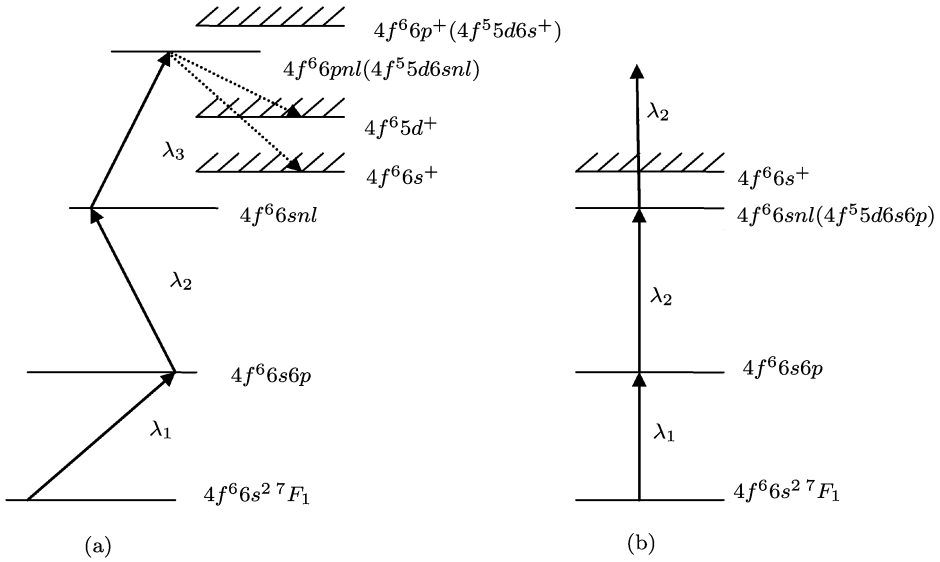


Fig.2. The excitation schemes used in the experiment. (a) For the autoionization detection method, the wavelength of the first laser is fixed at $4f^6 6s^2 \rightarrow 4f^6 6s6p$ resonance transition, the wavelength of the third laser is fixed at near the resonance line of $4f^6 6s^+ \rightarrow 4f^6 6p^+$ or $4f^6 6s^+ \rightarrow 4f^5 5d6s^+$, while the wavelength of the second laser is scanned to excite the atoms to $4f^6 6snl$ (l = 0, 2) Rydberg states. (b) For the direct photoionization detection method, the wavelength of the first laser is fixed at $4f^6 6s^2 \rightarrow 4f^6 6s6p$ resonance transition, the wavelength of the second laser is scanned to excite the atoms to $4f^6 6snl$ (l = 0, 2) Rydberg states and doubly excited $4f^5 5d6s6p$ valence states, then these states are ionized by the second photon of the second laser.

A schematic diagram of the relevant energy levels is shown in Fig.2. When the autoionization detection is used, one must reduce the intensity of the second laser to ensure that no signal appears while blocking the third laser. The excitation scheme used here is the so-called isolated-core excitation (ICE).[26] As shown in Fig.2(a), the third laser drives mainly the core resonance transition $4f^6 6s^+ \rightarrow 4f^6 6p^+$ or $4f^6 6s^+ \rightarrow$

$4f^5 5d6s^+$ to reach the $4f^6 6pnl$ or $4f^5 5d6snl$ autoionizing states. In other words, the third laser does not ionize the atom in the valence states, unless they are strongly mixed with $4f^6 6snl$ Rydberg states. In the experiment, the pulse of the third laser has a 10 ns delay relative to that of the second laser, which ensures that atoms already exist in the $4f^6 6snl$ states made by the first two lasers before they arrive at the interaction region. On the other hand, in the case where direct photoionization detection is used as shown in Fig.2(b), the intensity of the second laser must be enhanced in order to ionize the Rydberg states and valence states simultaneously.

In order to ensure the accuracy of the experimental data, some errors, such as the non-linearity in wavelength scans, have been corrected. Specifically, a hollow cathode lamp and a Fabry–Perot etalon are employed to calibrate the wavelength of lasers; to reduce the random errors in the spectra, each spectrum is measured several times. On the other hand, it is important to control the power of the third laser to avoid the power-broadening effect, which is crucial to the width measurement of an autoionizing state.

3. Results and discussion

As mentioned above, in order to investigate the highly excited even-parity states of the Sm atom systematically, both the autoionization detection method and the direct photoionization detection method are employed in this work. Comparisons of the spectra obtained using the two methods enable us to discriminate the Rydberg states from the valence states in the same energy region. Futhermore, with the electric-dipole selection rules for total angular momentum J, the possible values of J are also assigned to these states.

In the experiment, in order to confirm the feasibility of the autoionization detection method, and to choose the most appropriate wavelength of the third laser, we investigate the $4f^6 6pnl$ and $4f^5 5d6snl$ autoionization spectra relevant to the corresponding Rydberg states. An example of the observed spectra is shown in Fig.3, which is obtained by scanning the wavelength of the third laser across the core resonance transition $4f^6 6s^+ J = 1/2 \rightarrow 4f^6 6p^+ J = 3/2$, while the wavelengths of the first two lasers are set to populating the $4f^6 6snl$ Rydberg state.

Determining the values of n and l of the $4f^6 6pnl$ autoionizing state shown in Fig.3 requires information on the atomic wavefunctions, thus it is helpful to estimate the value of n. This can be done as follows. Due to the application of ICE, the n value of the $4f^6 6pnl$ autoionizing state shown in Fig.3 is the same as that of the $4f^6 6snl$ Rydberg state; The quantum defects Δ of many $4f^6 6snl$ Rydberg states in a Rydberg series should roughly be a constant. Based on the calculations of the effective principal quantum number n^* for many $4f^6 6s7s$ Rydberg states,[25] their values of Δ are between 4.23 and 4.45. A similar calculation indicates that $\Delta = 4.36$ with $n = 8$ for the $4f^6 6snl$ Rydberg state, from which the spectrum of the $4f^6 6pnl$ autoionizing state shown in Fig.3 is obtained. In other words, the observed spectrum shown in Fig.3 represents the transition from the $4f^6 6s8l$ state to the $4f^6 6p8l$ state.

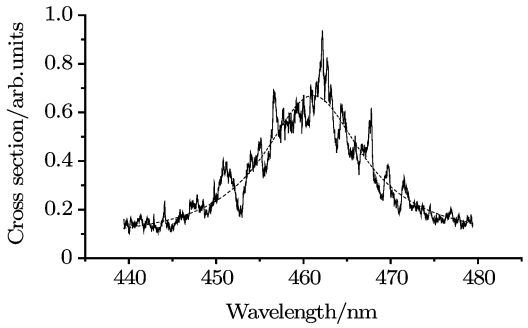


Fig.3. Observed autoionization spectrum for the $4f^6 6pnl$ state. It is obtained by scanning the wavelength of the third laser across the $4f^6 6s^+ \quad J{=}1/2 \rightarrow 4f^6 6p^+ \quad J{=}3/2$ core resonance transition, while the wavelengths of the first two lasers are set to populating the $4f^6 6snl$ Rydberg state. The abscissa represents the wavelength of the third laser, the dashed line represents the best fit from the Lorentzian-profile-fitting procedure.

On the other hand, the application of ICE greatly simplifies the autoionization spectrum from a Fano profile to a Lorentzian profile. As shown in Fig.3, the peak position and width can be easily extracted by a Lorentzian-profile-fitting procedure, and are 461.10 nm and 13.79 nm, respectively. For other autoionizing states with different n values observed in the present work, their spectra also have Lorentzian profiles. This indicates that the Rydberg electron, far from the ionic core, acts like a spectator during the core transition $4f^6 6s^+ J = 1/2 \rightarrow 4f^6 6p^+ J = 3/2$, as the excitation of the Rydberg electron to the continuum states is negligible. That is, the detection laser only drives the core $4f^6 6s^+ J = 1/2 \rightarrow 4f^6 6p^+ J = 3/2$ resonance transition of the Sm atom in this step. Since the outer nl electron only acts like a specta-

tor during the excitation, the frequency only shifts slightly from the core transition. For example, in the spectrum shown in Fig.3, the location of the peak is 0.32 nm red-shifted from the core transition $4f^6 6s^+ J = 1/2 \rightarrow 4f^6 6p^+ J = 3/2$. Note that the shift from the ion transition line is very small as compared with the width of a resonance for most autoionizing states.

Obviously, the autoionization detection efficiency should be proportional to the total cross section of autoionization, whose peak matches the wavelegth corresponding to the maximum of detection efficiency. Thus, an ideal detection efficiency may be obtained by adjusting the wavelength of the detecting laser near the resonance peak. On the other hand, a large width of the autoionizing state enables us to conveniently adjust the wavelength of the laser as it is not so sensitive. A spectrum of the even-parity Rydberg states is shown in Fig.4 as an example of autoionization detection. It is obtained by fixing the wavelength of the third laser at 461.10 nm, where the abscissa represents the energy of the second laser in wave numbers (cm^{-1}).

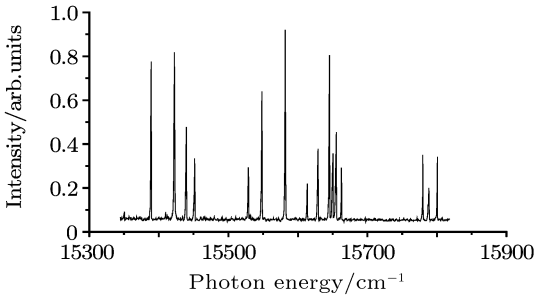


Fig.4. An example of the experimental spectra for the Sm atom with the autoionization detection method. It is obtained by scanning the wavelength of the second laser over a broad spectral range while the wavelengths of the first and third lasers are fixed at proper values.

In the process of obtaining this Rydberg spectrum, one must reduce the intensity of the second laser to ensure that no signal appears while blocking the third laser. For each Rydberg state, an autoionizing state can be observed by scanning the wavelength of the third laser across the core resonance transition $4f^6 6s^+ \rightarrow 4f^6 6p^+$ or $4f^6 6s^+ \rightarrow 4f^5 5d 6s^+$. In addition, we carefully control the experimental settings in order to obtain information about the relative intensity of spectral lines simultaneously, which plays an important role in providing information about the spectra.

On the other hand, only the first two lasers are used when the spectra are measured with the direct photoionization detection method. In this case, the second laser is also used as a detecting laser after it excites the Rydberg states. Furthermore, the intensity of the second laser must be enhanced in order to ionize the Rydberg states and valence states simultaneously. An example of many such measurements is shown in Fig.5, where the wavelength of the second laser is scanned in the same energy range as in Fig.4.

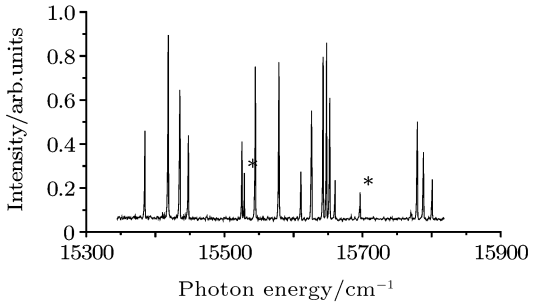


Fig.5. An example of the experimental spectra for the Sm atom with the direct photoionization detection method. It is obtained by scanning the wavelength of the second laser while the wavelength of the first laser is fixed at the $4f^6 6s^2 \rightarrow 4f^6 6s 6p$ resonance transition. The valence states are marked with asterisks.

Comparison of Figs.4 and 5 may indicate the difference between the two detection methods. The two peaks, marked with asterisks in Fig.5, can be identified as the two valence states, as they do not exist in Fig.4, and can be further confirmed by blocking the beam of the first laser. With this principle, a large number of valence states are observed in this work. Although the various laser dyes used in this experiment cover different wavelength regions, there are sufficient overlaps between them. The continuity in wavelength allows us to systematically detect the high-lying energy levels with both the autoionization detection and direct photoionization detection methods.

The information on the highly excited states obtained in this work can be found in the following tables. Tables 1–3 list the data for the Rydberg states, while Tables 4–6 provide the information for the valence states. Note that the energy of the highly excited state is obtained by adding the energy of the chosen intermediate state to the corresponding photon energy of the second laser. The typical experimental uncertainties are estimated to be less than ± 0.1 cm^{-1}. The relative intensities are normalized and then classified into weak, medium and strong, representing the three ranges: 0–0.3, 0.3–0.6 and 0.6–1. They are marked in all tables by symbols W, M and S, respectively.

Table 1. The level energies, relative intensities and possible J values of even-parity Rydberg states obtained in this experiment. The level energies and the possible J values reported in Refs.[16] and [18] are also listed for comparison. The typical experimental uncertainties are estimated to be less than ± 0.1 cm^{-1}, and the relative intensities are normalized and classified into three ranges: 0–0.3, 0.3–0.6 and 0.6–1, marked by W, M and S, respectively.

serial number	energy/cm^{-1}	intensity	total angular momentum (J)	previous data*/cm^{-1}
1	36362.41	M	2	36362.26
2	36364.17	M	3	36363.98
3	36377.20	S	1	36377.10
4	36403.89	S	1	36403.90
5	36409.32	S	3	36409.36
6	36474.63	W	2	36474.52
7	36515.39	M	2	36515.30
8	36536.80	M	1,3	36536.70[a]
9	36565.28	M	1	36565.30
10	36572.09	S	3	36572.30
11	36587.27	M	3	36587.50
12	36592.71	M	2	36592.80[a]
13	36618.88	M	2	36619.00
14	36628.64	M	1	36628.68
15	36644.59	S	1	36644.41
16	36682.57	M	3	36682.46
17	36964.49	W	2	36964.20[a]
18	36976.05	W	2	36976.10
19	36996.47	M	3	36996.55
20	37029.69	W	1	37029.70
21	37054.67	W	3	37054.40[a]
22	37066.97	M	2,3	37067.00[a]
23	37070.62	S	1	37070.63
24	37130.03	W	2,3	37130.10[a]
25	37164.76	M	1,2	37164.71
26	37171.15	M	1	37171.11
27	37174.78	M	2	37175.00[a]
28	37214.00	S	2	37213.83
29	37244.26	S	3	37244.50[a]
30	37269.95	S	1,2	37269.89
31	37339.81	S	1	37339.91
32	37357.01	S	1,2	37356.75
33	37387.03	S	1,2	37386.92
34	37416.26	W	1	37416.23
35	37430.18	M	1	37430.19
36	37449.79	S	2	37449.69
37	37493.90	M	1	37493.87
38	37568.71	S	3	37568.81
39	37576.70	S	2	37576.70
40	37616.39	W	3	37616.50
41	37629.81	W	2	37629.72
42	37679.60	M	1	37679.39
43	37708.32	S	1	37708.10
44	37812.31	M	1	37812.31
45	37815.00	S	3	37814.90[a]
46	37826.07	W	1,2	37825.95
47	37943.93	S	1	37944.03
48	37971.24	M	2	37971.15
49	38084.70	S	2	38084.57
50	38109.35	W	2	38109.25

Table 1. (*Continued*).

serial number	energy/cm^{-1}	intensity	total angular momentum (J)	previous data*/cm^{-1}
51	38147.44	W	2	38147.42
52	38292.08	W	1	38292.26
53	38317.02	M	2	38316.89
54	38382.14	S	2	38381.99
55	38413.44	M	2	38413.39
56	38421.71	W	1	38421.68
57	38482.40	W	2	38482.14
58	38505.80	M	1	38505.77
59	38591.58	S	3	38591.41
60	38633.97	S	3	38633.92
61	38673.42	S	1	38673.42
62	38700.16	S	2	38700.08
63	38733.99	S	3	38733.78
64	38738.29	S	1	38738.30
65	38760.37	S	3	38760.16
66	38763.79	M	3	38763.65
67	38818.33	S	2	38818.18
68	38883.44	W	3	38883.26
69	38890.87	W	2	38890.85
70	38966.69	W	2	38966.55
71	39182.69	M	1	39182.50
72	39243.83	W	2	39243.54
73	39246.31	M	1	39246.05
74	39301.25	S	2	39301.07
75	39309.79	S	2	39309.53
76	39471.54	S	2	39471.68
77	39496.07	S	3	39496.00
78	39521.85	M	3	39522.08
79	39538.42	S	3	39538.28
80	39548.37	W	1	39548.10
81	39590.38	S	1	39590.35
82	39626.88	S	1	39626.70
83	39648.40	S	3	39648.30
84	39673.63	S	1	39673.50
85	39961.66	W	1	39961.52
86	39970.08	S	2	39969.85

*The previous data marked with 'a' are taken from Ref.[18]; the remainder are taken from Ref.[16].

It is necessary to point out that although the Rydberg states shown in Table 1 were obtained previously,[16,18] they could not be identified from the valence states in the same energy region. In this work, however, the advantage of autoionization detection enables us to discriminate them successfully from the valence states. The corresponding values in previous studies[16,18] are also tabulated in Table 1 for handy comparison. Our data show a good agreement within the uncertainties with them, where the experiment was carried out with a two-step photoexcitation and photoionization method. Moreover, in previous work the information about the relative intensities of the spectral lines cannot be found, which plays an important role in analyzing the features of the spectra. In addition, much effort is also made to determine the possible values for the total angular momentum J of these states, with the knowledge of selection rules for J under the electric-dipole approximation. Therefore, the present work not only confirms the observations in the literature, but also assigns unique J values to the Rydberg states in Table 2. The assignments are based on the comparison between the present work and previous work,[16] removing the ambiguity there on the possible J values.

Table 2. The level energies, relative intensities and the possible J values of even-parity Rydberg states obtained in this experiment. The possible J values of these states reported in Ref.[16] are determined as 3 or 4. The typical experimental uncertainties are estimated to be less than ± 0.1 cm^{-1}, and the relative intensities are normalized and classified into three ranges: 0–0.3, 0.3–0.6 and 0.6–1, marked by W, M and S, respectively.

serial number	energy/cm^{-1}	intensity	total angular momentum (J)	previous data*/cm^{-1}
1	37717.75	M	3	37717.71
2	37879.76	S	3	37879.80
3	38035.41	W	3	38035.59
4	38043.97	M	3	38043.78
5	38463.80	M	3	38463.60
6	40037.18	S	3	40036.94
7	40366.94	W	3	40367.20

*The previous data are taken from Ref.[16].

The possible J values of the Rydberg states listed in Table 2 should be 1, 2 or 3 according to the electric-dipole selection rules for the excitation scheme (a) described in Fig.2, which were determined as 3 or 4 in earlier work.[16] Therefore, these states must have the value of $J = 3$, based on a comparison of the two different excitation schemes used.

Table 3. The level energies, relative intensities and possible J values of even-parity new Rydberg states obtained in this experiment. The typical experimental uncertainties are estimated to be less than ± 0.1 cm^{-1}, and the relative intensities are normalized and classified into three ranges: 0–0.3, 0.3–0.6 and 0.6–1, marked by W, M and S, respectively.

serial number	energy/cm^{-1}	intensity	total angular momentum (J)
1	36455.63	M	1,2,3
2	37042.07	W	1,2,3
3	37259.25	S	1,2,3
4	37454.16	S	1,2,3
5	37460.97	M	1,2,3
6	37561.04	W	1,2,3
7	37610.44	W	1,2,3
8	37641.45	S	1,2,3
9	37899.58	S	1,2,3
10	37909.81	S	1,2,3
11	37922.44	W	1,2,3
12	37998.52	M	2,3
13	38025.13	W	1,2,3
14	38364.62	M	1,2,3
15	38391.56	S	1,2,3
16	38432.09	M	1,2,3
17	38853.56	S	1,2,3
18	39312.85	W	1
19	39455.20	W	1
20	40271.40	W	1
21	40389.77	M	1
22	40431.77	W	2,3
23	40473.08	W	2,3
24	40611.64	W	2,3
25	40616.58	W	2,3
26	40641.37	W	2,3
27	40713.61	W	2,3
28	40736.85	W	2,3
29	40798.65	M	1,2,3

Using excitation schemes different from that used in previous work,[16] spectral information, including level energies, relative intensities and possible J values, on the 29 new Rydberg states in the same energy region is obtained, as shown in Table 3. Two possible reasons can explain why they could not be found in the previous photoionization experiment: firstly, different excitation schemes were used there,[16] leading to an intermediate state not accessible to the states shown in Table 3; secondly, unlike the previous experiment carried out with a two-step photoexcitation and photoionization, a three-step autoionization detection method is employed here. It is well known that autoionization detection has a much higher efficiency than direct photoionization detection for the same Rydberg state. Furthermore, the ionization efficiency of the direct photoionization detection method is inversely proportional to the energy difference $\Delta E = E_1 - E_i$, where E_1 is the total energy of the three photons and E_i is the first ionization limit. Obviously, as the wavelength of the second laser is tuned towards the blue direction, the increase of ΔE certainly reduces the ionization efficiency for the Rydberg states. However, with the autoionization detection method, the ionization efficiency is almost the same for all the Rydberg states, as the wavelength of the third laser can be tuned at the resonance transition, $4f^6 6s^+ \rightarrow 4f^6 6p^+$ or $4f^6 6s^+ \rightarrow 4f^5 5d 6s^+$, of the core electron. The present experiment confirms the above expectation by effectively detecting the Rydberg states in a wide energy range.

Now, we turn to discuss the valence states in Tables 4–6, which are discriminated from the Rydberg states in the same energy region by comparing the spectra obtained from the two detection methods.

Table 4. The level energies, relative intensities and the possible J values of even-parity valence states obtained in this experiment. The level energies and the possible J values reported in Ref.[16] are also listed for comparison. The typical experimental uncertainties are estimated to be less than ± 0.1 cm^{-1}, and the relative intensities are normalized and classified into three ranges: 0–0.3, 0.3–0.6 and 0.6–1, marked by W, M and S, respectively.

serial number	energy/cm^{-1}	intensity	total angular momentum (J)	Previous data*/cm^{-1}
1	36391.30	M	2	36391.26
2	37342.99	W	3	37342.75
3	37967.82	S	1	37967.60
4	38128.57	M	2	38128.30
5	38608.44	S	2	38608.50
6	38774.08	W	3	38774.00
7	38793.29	M	3	38793.35
8	39106.00	W	2	39105.75
9	39154.38	W	3	39154.09
10	39171.34	M	2	39171.10
11	39182.65	W	1	39182.50
12	39215.81	W	1	39215.56
13	39227.29	M	2	39227.10
14	39246.30	W	1	39246.05
15	39272.49	W	3	39272.30
16	39281.03	W	1	39280.88
17	39346.91	M	2	39346.85
18	39538.81	W	1	39538.58
19	39559.81	W	3	39559.60
20	39590.54	M	1	39590.35
21	39597.60	M	2	39597.36
22	39615.38	W	3	39615.20
23	39626.91	M	1	39626.70
24	39673.64	S	1	39673.50
25	39751.46	M	2	39751.26
26	39794.11	S	2	39793.90
27	39797.87	S	1	39797.65
28	39828.44	M	2	39828.30
29	39896.49	S	2	39896.25
30	39901.27	S	1	39901.02
31	39927.03	W	2	39926.75
32	39958.29	S	2	39958.00
33	40761.60	W	2	40761.56

*The previous data are taken from Ref.[16].

Similar to the spectral data listed in Table 1, the states listed in Table 4 were observed previously without any identification: valence states or Rydberg states. For a handy comparison, the level energies from both the present and previous works are tabulated in Table 4, and are in good agreement within the experimental uncertainties. Just like the case of Rydberg states, the information on relative intensities of valence states is also reported, which is not available in the literature. In addition, this work assigns unique J values to the valence states in Table 5.

Table 5. The level energies, relative intensities and possible J values of even-parity valence states obtained in this experiment. The possible J values of these states reported in Ref.[16] are determined as 3 or 4. The typical experimental uncertainties are estimated to be less than ± 0.1 cm^{-1}, and the relative intensities are normalized and classified into three ranges: 0–0.3, 0.3–0.6 and 0.6–1, marked by W, M and S, respectively.

serial number	energy/cm^{-1}	intensity	total angular momentum (J)	previous data*/cm^{-1}
1	37904.32	W	3	37904.36
2	38121.95	W	3	38122.13
3	38406.28	M	3	38406.20
4	40366.95	W	3	40367.20
5	40514.85	W	3	40514.90

*The previous data are taken from Ref.[16].

Similar to the J values of the Rydberg states listed in Table 2, the possible J values of the valence states listed in Table 5 should be 1, 2 or 3 according to the knowledge of electric-dipole selection rules for the excitation scheme (a) used in this work, which were determined as 3 or 4 in earlier work.[16] Therefore, these states must have the value of $J = 3$, based on a comparison of the two different excitation schemes used.

Table 6. The level energies, relative intensities and possible J values of even-parity new valence states obtained in this experiment. The typical experimental uncertainties are estimated to be less than ± 0.1 cm^{-1}, and the relative intensities are normalized and classified into three ranges: 0–0.3, 0.3–0.6 and 0.6–1, marked by W, M and S, respectively.

serial number	energy/cm^{-1}	intensity	total angular momentum (J)
1	38106.51	W	1,2,3
2	38398.44	W	1,2,3
3	38469.32	W	1,2,3
4	39095.91	M	2,3
5	39112.38	W	2,3
6	39210.53	W	2,3
7	39339.53	S	2,3
8	39391.29	W	2,3
9	39455.26	W	1
10	39955.23	W	2,3
11	40086.83	W	1
12	40132.08	W	1
13	40349.26	W	1
14	40483.74	S	2,3
15	40488.44	S	1
16	40587.28	M	1
17	40645.27	W	2,3
18	40661.59	M	1
19	40687.53	W	2,3
20	40724.68	W	2,3
21	40775.61	W	2,3
22	40781.72	W	2,3
23	40791.08	M	1

Using excitation schemes different from that used in previous work,[16] spectral information on 23 new valence states, including level energies, relative intensities and possible J values, is obtained in the same energy region, as listed in Table 6. A possible reason why they could not be found in the previous work is that the transition of the second step, from the intermediate state to the new valence state, is forbidden for the excitation scheme used in the lierature. In addition, using the excitation scheme (b) only the $J = 1$ states can be reached, hence some states can be assigned only one J. For other states two or three possible J can be given, based on a comparison of the two different excitation schemes employed in this work.

Finally, as shown in Tables 1–6, 183 energy levels have been observed in the energy region between 36360 cm^{-1} and 40800 cm^{-1}. In the same energy region, 246 energy levels were reported in previous studies,[16,18] using the two-color three-photon ionization method. Among these experimental data, 131 energy levels are common. Comparison of our data with those obtained in previous work shows that they are in good agreement. However, the spectral information, including level energies, relative intensities and possible J values, for the 52 new states in the same energy region has never been reported in previous work. Therefore, in order to have a complete information on the Sm atom, excitation schemes and methods different from previous studies are necessary, as have been described in this paper.

4. Conclusion

A systematic study on the highly excited even-parity states of the Sm atom has been carried out with the three-step autoionization detection method and direct photoionization detection method in the energy region between 36360 cm^{-1} and 40800 cm^{-1}. With the information on level energies, possible J values and their relative intensities, the Rydberg states are discriminated from the valence states in the same energy region by comparing the spectra from the two detection methods. In the experiment two different excitation schemes are designed to obtain the spectra of highly excited even-parity states of the Sm atom. With a detailed analysis of the experimental data, this work not only confirms the results about many spectral data from the literature with different excitation schemes, but also assigns unique J values to some of the energy levels, removing the ambiguity in the previous work. Moreover, more than 50 new spectral data, including Rydberg states and valence states, are reported in this work. The experimental results not only greatly enrich the spectral information on the Sm atom, but also futher confirm that autoionization detection is an effective method for the study of Rydberg states of a rare-earth atom.

References

[1] Fedoseev V N, Mishin V I, Vedeneev D S and Zuzikov A D 1991 *J. Phys.* B: *At. Mol. Opt. Phys.* **24** 1575
[2] Camus P, De'barre A and Morillon C 1980 *J. Phys.* B: *At. Mol. Opt. Phys.* **13** 1073
[3] Smith G and Tomkins F S 1975 *Proc. R. Soc. Lond.* A **342** 149
[4] Jones R R 1998 *Phys. Rev.* A **58** 2608
[5] Camus P, Dieulin M and EI Himdy A 1982 *Phys. Rev.* A **26** 379
[6] Tran N H, Pillet P, Kachru R and Gallagher T F 1984 *Phys. Rev.* A **29** 2640
[7] Dai C J 1995 *Phys. Rev.* A **52** 4416
[8] Lange V, Eichmann U and Sandner W 1989 *J. Phys.* B: *At. Mol. Opt. Phys.* **22** L245
[9] Whitfield S B, Caspary K, Wehlitz R and Martins M 2008 *J. Phys.* B: *At. Mol. Opt. Phys.* **41** 015001
[10] Nakhate S G, Razvi M A N, Connerade J P and Ahmad S A 2000 *J. Phys.* B: *At. Mol. Opt. Phys.* **33** 5191
[11] Vidolova-Angelova E P, Krustev T B, Angelov D A and Mincheva S 1997 *J. Phys.* B: *At. Mol. Opt. Phys.* **30** 667
[12] Xu C B, Xu X Y, Huang W, Xue M and Chen D Y 1994 *J. Phys.* B: *At. Mol. Opt. Phys.* **27** 3905
[13] Dai C J, Zhang S, Shu X W, Fang D W and Li J 1995 *J. Quant. Spectrosc. Radiat. Transfer* **53** 179
[14] Yi J H, Lee J and Kong H J 1995 *Phys. Rev.* A **51** 3053
[15] Jayasekharan T, Razvi M A N and Bhale G L 1996 *J. Opt. Soc. Am.* B **13** 641
[16] Jayasekharan T, Razvi M A N and Bhale G L 2000 *J. Opt. Soc. Am.* B **17** 1607
[17] Jayasekharan T, Razvi M A N and Bhale G L 2000 *J. Phys.* B: *At. Mol. Opt. Phys.* **33** 3123
[18] Gomonai A I and Plekan O I 2003 *J. Phys.* B: *At. Mol. Opt. Phys.* **36** 4155
[19] Dai C J and Zhao X A 1995 *J. Quant. Spectrosc. Radiat. Transfer* **54** 1019
[20] Lu J, Dai C J, Li C Q, Xu X H, Liu Z D and Tang J C 1999 *J. Quant. Spectrosc. Radiat. Transfer* **61** 339
[21] Lu J, Dai C J, Xu Y F and Li S B 2001 *Chin. Phys. Lett.* **18** 1192
[22] Hang W, Xu X Y, Xu C B, Xue P, Xue M and Chen D Y 1996 *Phys. Rev.* A **54** 5423
[23] Cheng C H and Gallagher T F 2000 *Phys. Rev.* A **61** 063411
[24] Li S B and Dai C J 2004 *J. Electron Spectrosc. Relat. Phenom.* **136** 247
[25] Martin W C, Zalubas R and Hagan L 1978 *Atomic Energy Levels—The Rare-Earth Elements* (Washington: U.S. Government Printing Office) p162
[26] Cook W E, Gallagher T F, Edelstein S A and Hill R M 1978 *Phys. Rev. Lett.* **40** 178